

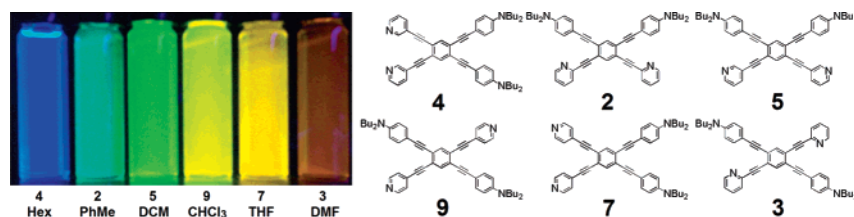
Systematic Structure–Property Investigations and Ion-Sensing Studies of Pyridine-Derivatized Donor/Acceptor Tetrakis(arylethynyl)benzenes

Eric L. Spitler, Laura D. Shirtcliff, and Michael M. Haley*

Department of Chemistry and Materials Science Institute, University of Oregon,
Eugene, Oregon 97403-1253

haley@uoregon.edu

Received August 17, 2006



Nine structural isomers of a tetrakis(arylethynyl)benzene chromophore functionalized with dibutylaniline and pyridine units as respective donors and acceptors have been synthesized and their steady-state spectroscopic parameters investigated. The effects of small structural variations on the electronic absorption and emission spectra have been explored in evaluation of their potential as optical materials components. These structural variations have predictable consequences and thus allow fine-tuning of the optoelectronic properties for specialized applications. Strong solvatochromism is also displayed. Their response to protonation and metal ion complexation caused dynamic shifts in the emission spectra, providing evidence for a stepwise intramolecular charge-transfer switching phenomenon manifested by either hypsochromic or bathochromic shifts in the fluorescence λ_{max} . These shifts are believed to correlate strongly to the relative energies of the fluorophore's HOMO and LUMO levels. The complete array of compounds represents an interesting set of candidates for fluorescent sensing device components.

Introduction

Carbon-rich, highly conjugated organic molecules have been the subject of considerable study in recent years,¹ primarily because of their unique optoelectronic properties.^{2,3} These compounds are now recognized as ideal materials for advanced applications including organic light-emitting diodes, thin film organic transistors, solar cells, and optical storage devices.^{1–3} We recently presented detailed structure–property relationship investigations into donor/acceptor-substituted tetrakis(phenylethynyl)benzenes and related bis(dehydrobenzoannuleno)benzenes (Figure 1).⁴ These carbon-rich chromophores exhibit a

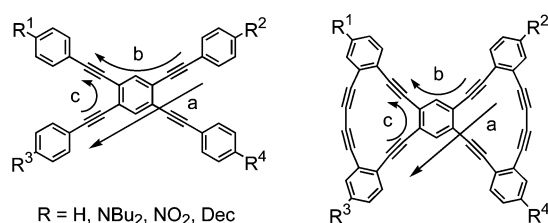


FIGURE 1. Conjugated pathways present in tetrakis(phenylethynyl)benzenes and structurally related bis(dehydrobenzoannuleno)benzenes.

high degree of conjugation and consequently possess multiple pathways for intramolecular electronic and photonic transfer. As a result, these molecules are excellent candidates for many of the optical materials applications mentioned above.^{3,5,6} Their electronic absorption and emission profiles exhibit sensitivity to functional group substitution pattern as well as solvent environment. These compounds also possess significant non-linear optical susceptibilities arising from the highly polarized

* To whom correspondence should be addressed. Tel: 541-346-0456. Fax: 541-346-0487.

(1) (a) de Meijere, A., Ed. *Top. Curr. Chem.* (Carbon Rich Compounds I); Springer: Berlin, 1998; Vol. 196. (b) de Meijere, A., Ed. *Top. Curr. Chem.* (Carbon Rich Compounds II); Springer: Berlin, 1999; Vol. 201. (c) Diederich, F., Stang, P. J., Tykwinski, R. R., Eds. *Acetylene Chemistry: Chemistry, Biology, and Material Science*; Wiley-VCH: Weinheim, 2005. (d) Haley, M. M., Tykwinski, R. R., Eds. *Carbon-Rich Compounds: From Molecules to Materials*; Wiley-VCH: Weinheim, 2006.

conjugation pathways between the electron-donating and -accepting groups.^{6a,g,h,7}

One intriguing facet of these studies is the effect of the relative strengths of the donor and/or acceptor groups on the optical properties. Studies on similar systems show that the degree of donating and/or accepting ability can significantly influence the electronic spectra.^{6g,h,8} An expanded continuation of our studies therefore involves varying not only the substitution pattern on the central benzene ring but also the identity of the functional groups on/in the peripheral arene rings. In particular, the effect of differing electron-accepting groups is of interest in determining structure–property relationships. Arylacetylenes have shown themselves amenable to “tuning” of electronic and optical properties by fundamental variations in the charge-transfer pathway as well as chemical environment.^{6a,g,h,8} In this paper, we examine the effect of a pyridyl group as the (weaker) electron acceptor in place of the previously reported nitrophenyl-functionalized systems.

Donor/acceptor properties in related phenyleneethynylene/vinylene cruciforms, including one that incorporates 4-substi-

(2) Reviews, inter alia: (a) *Organic Light Emitting Devices: Synthesis, Properties and Applications*; Müllen, K., Scherf, U., Eds.; Wiley-VCH: Weinheim, 2006. (b) Chen, J.; Reed, M. A.; Dirk, S. M.; Price, D. W.; Rawlett, A. M.; Tour, J. M.; Grubisha, D. S.; Bennett, D. W. In *NATO Science Series II: Mathematics, Physics, Chemistry (Molecular Electronics: Bio-Sensors and Bio-Computers)*; Plenum: New York, 2003; Vol. 96, pp 59–195. (c) Domercq, B.; Hreha, R. D.; Zhang, Y.-D.; Haldi, A.; Barlow, S.; Marder, S. R.; Kippelen, B. *J. Poly. Sci. Part B: Poly. Phys.* **2003**, *41*, 2726–2732. (d) Shirota, Y. *J. Mater. Chem.* **2000**, *10*, 1–25. (e) Schwab, P. F. H.; Levin, M. D.; Michl, J. *Chem. Rev.* **1999**, *99*, 1863–1933. (f) *Electronic Materials: The Oligomer Approach*; Müllen, K., Wegner, G., Eds.; Wiley-VCH: Weinheim, 1998. (g) *Nonlinear Optics of Organic Molecules and Polymers*; Nalwa, H. S., Miyata, S., Eds.; CRC Press: Boca Raton, 1997.

(3) Recent examples, inter alia: (a) Kang, H.; Evrenenko, G.; Dutta, P.; Clays, K.; Song, K.; Marks, T. J. *J. Am. Chem. Soc.* **2006**, *128*, 6194–6205. (b) Knox, J. E.; Halls, M. D.; Hratchian, H. P.; Schlegel, H. B. *Phys. Chem. Chem. Phys.* **2006**, *8*, 1371–1377. (c) Shukla, V. K.; Kumar, S.; Deva, D. *Synth. Met.* **2006**, *156*, 387–391. (d) Seminario, J. M. *Nature Mater.* **2005**, *4*, 111–113. (e) Hughes, G.; Bryce, M. R. *J. Mater. Chem.* **2005**, *15*, 94–107. (f) Van der Auweraer, M.; De Schryver, F. C. *Nature Mater.* **2004**, *3*, 507–508. (g) Special Issue on “Organic Electronics”. *Chem. Mater.* **2004**, *16*, 4381–4846. (h) Simpson, C. D.; Wu, J.; Watson, M. D.; Müllen, K. *J. Mater. Chem.* **2004**, *14*, 494–504.

(4) (a) Marsden, J. A.; Miller, J. J.; Shirtcliff, L. D.; Haley, M. M. *J. Am. Chem. Soc.* **2005**, *127*, 2464–2476. See also: (b) Marsden, J. A.; Haley, M. M. *Angew. Chem., Int. Ed.* **2004**, *43*, 1694–1697. (c) Miller, J. J.; Marsden, J. A.; Haley, M. M. *Synlett* **2004**, 165–168.

(5) (a) Bunz, U. H. F.; Rubin, Y.; Tobe, Y. *Chem. Soc. Rev.* **1999**, 107–119. (b) Haley, M. M.; Wan, W. B. In *Advances in Strained and Interesting Organic Molecules*; Halton, B., Ed.; JAI Press: Greenwich, 2000; Vol. 8, pp 1–41. (c) Watson, M. D.; Fechtenkötter, A.; Müllen, K. *Chem. Rev.* **2001**, *101*, 1267–1300. (d) Nielsen, M. B.; Diederich, F. In *Modern Arene Chemistry*; Astruc, D., Ed.; Wiley-VCH: Weinheim, 2002; pp 196–216.

(6) Inter alia: (a) Zhao, Y.; Slepokov, A. D.; Akoto, C. O.; McDonald, R.; Hegmann, F. A.; Tykwinski, R. R. *Chem. Eur. J.* **2005**, *11*, 321–329. (b) Bunz, U. H. F. *Adv. Polym. Sci.* **2005**, *177*, 1–52. (c) Fasina, T. M.; Collings, J. C.; Lydon, D. P.; Albesa-Jove, D.; Batsanov, A. S.; Howard, J. A. K.; Nguyen, P.; Bruce, M.; Scott, A. J.; Clegg, W.; Watt, S. W.; Viney, C.; Marder, T. B. *J. Mater. Chem.* **2004**, *14*, 2395–2404. (d) Boydston, A. J.; Yin, Y.; Pagenkopf, B. L. *J. Am. Chem. Soc.* **2004**, *126*, 3724–3725. (e) Gonzalo-Rodríguez, J.; Esquivias, J.; Lafuente, A.; Diaz, C. *J. Org. Chem.* **2003**, *68*, 8120–8128. (f) Bunz, U. H. F. *Chem. Rev.* **2000**, *100*, 1605–1644. (g) Tykwinski, R. R.; Gubler, U.; Martin, R. E.; Diederich, F.; Bosshard, C.; Günter, P. *J. Phys. Chem. B* **1998**, *102*, 4451–4465. (h) Tykwinski, R. R.; Schreiber, M.; Carlón, R. P.; Diederich, F.; Gramlich, V. *Helv. Chim. Acta* **1996**, *79*, 2249–2280.

(7) (a) Slepokov, A.; Marsden, J. A.; Miller, J. J.; Shirtcliff, L. D.; Haley, M. M.; Kamada, K.; Tykwinski, R. R.; Hegmann, F. A. In *Nonlinear Optical Transmission and Multiphoton Processes in Organics III*; Proc. SPIE **2005**, *5934*, 29–34. (b) Slepokov, A.; Hegmann, F. A.; Tykwinski, R. R.; Kamada, K.; Ohta, K.; Marsden, J. A.; Spitzer, E. L.; Miller, J. J.; Haley, M. M. *Opt. Lett.* **2006**, *31*, 3315–3317. (c) Zhang, X.-B.; Feng, J.-K.; Ren, A.-M.; Sun, C.-C. *Opt. Mater.*, in press.

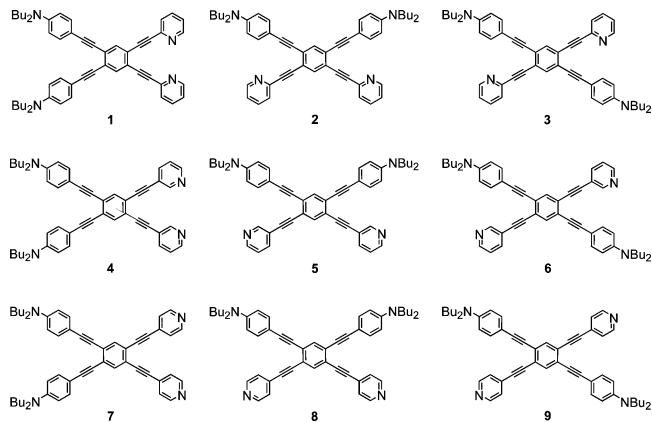


FIGURE 2. Isomeric donor/acceptor tetrakis(arylethynyl)benzene targets with pyridine acceptors.

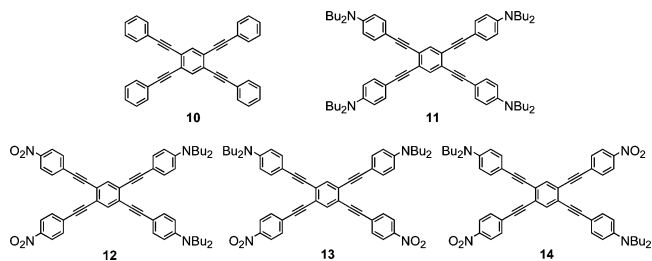
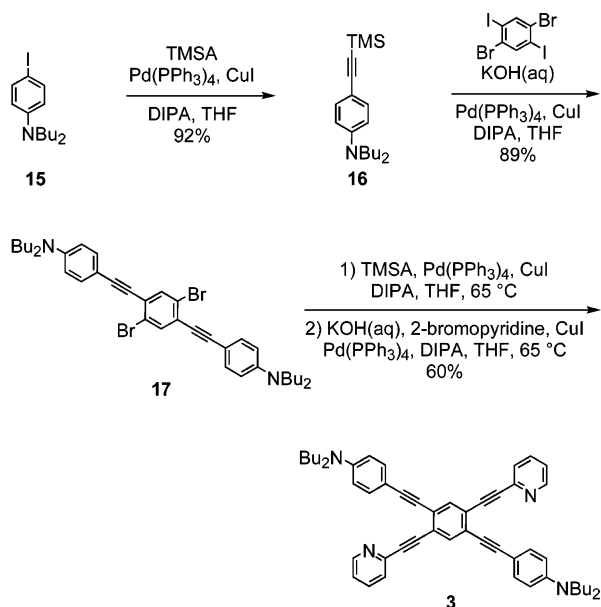


FIGURE 3. Previously reported tetrakis(phenylethynyl)benzenes **10–14**.

tuted pyridines, have been studied recently by Bunz et al.⁹ and have been shown, in addition to possessing unique optical properties, to exhibit exciting potential for selective ion sensing via intramolecular charge-transfer switching.¹⁰ The range of possible compounds expands greatly with variation not only of the ethynylpyridine substitution pattern (three substitution isomers) but also the position of the nitrogen atom within the ring relative to the acetylenic linker (three possible positions). Preparation of all nine permutations of the donor/acceptor-functionalized tetrakis(arylethynyl)benzenes (TAEBs) should permit a systematic study of the effects of small structural variations on the charge-transfer pathways as well as the overall materials properties of each system, and could potentially lead to customization of optical band gaps for specialized materials applications. Herein we present the syntheses and spectrophotometric studies of a family of pyridine-based donor/acceptor TAEBs (**1–9**, Figure 2) and comparison with the known nonfunctionalized parent (**10**), tetradonor (**11**), and nitrophenyl acceptor analogues (**12–14**, Figure 3).⁴ We also report our initial investigations into proton-induced and metal ion complexation-induced electronic spectra shifts. In all cases, we retain the *N,N*-dibutylaniline moiety as the electron donor unit.

(8) (a) Bazan, G. C.; Bartholomew, G. P. *J. Am. Chem. Soc.* **2002**, *124*, 5183–5196. (b) Bazan, G. C.; Bartholomew, G. P. *Synthesis* **2002**, 1245–1255. (c) Nguyen, P.; Lesley, G.; Marder, T. B. *Chem. Mater.* **1997**, *9*, 406–408. (d) Meier, H.; Mühlhng, B.; Kolshorn, H. *Eur. J. Org. Chem.* **2004**, 1033–1042. (e) Meier, H.; Gerold, J.; Kolshorn, H.; Mühlhng, B. *Chem. Eur. J.* **2004**, *10*, 360–370.

(9) (a) Wilson, J. N.; Bunz, U. H. F. *J. Am. Chem. Soc.* **2005**, *127*, 4124–4125. (b) Zuccherro, A. J.; Wilson, J. N.; Bunz, U. H. F. *J. Am. Chem. Soc.* **2006**, *128*, 11872–11881. (c) Wilson, J. N.; Josowicz, M.; Wang, Y. Q.; Bunz, U. H. F. *Chem. Commun.* **2003**, 2962–2963.

SCHEME 1. Representative Synthesis of Pyridine-Based Donor/Acceptor TAEBs

Results and Discussion

Synthesis. The general synthetic strategy for tetrakis(aryl-ethynyl)benzenes **1–9**, as previously reported in our extensive work on annulenes¹¹ and benzenes **10–14**,^{4a,c} relies on successive Pd-catalyzed Sonogashira cross-coupling reactions (Scheme 1).¹² Donor and acceptor segments are attached to a central tetrahalobenzene ring in a stepwise fashion that takes advantage of the electronic preferences of the catalytic cycle, as well as the reactivity difference between aryl bromides and aryl iodides toward cross-coupling.¹² Specifically, Sonogashira reaction of *N,N*-dibutyl-4-iodoaniline **15** with trimethylsilylacetylene (TMSA) affords **16**.^{4a} In situ desilylation under basic conditions¹³ and 2-fold cross-coupling of the “donor” alkyne to an isomer of dibromo-diiodobenzene furnishes one of three key intermediates (e.g., **17**). Reaction at room temperature allows selective coupling to the more reactive iodides to yield **17**. TMSA is then coupled to the bromine positions on the central ring at elevated temperatures to overcome the electronic unfavorability of an electron-rich arene toward the Sonogashira reaction. The product is an electron-rich alkyne, which is activated toward the final step, 2-fold coupling of bromopyridine, an electron-poor arene, to yield **3**. All nine regioisomers are readily obtained in this manner.

Although the final cross-coupling should be electronically favored, yields of the products (Table 1) have proven variable. This can potentially be explained by complexation of the Pd or Cu catalysts to the pyridine nitrogens. In particular, compounds in which the pyridine rings are *ortho* to each other have the potential for bidentate chelation, which could complicate the workup. Also, ¹H NMR spectra of insufficiently purified samples of products invariably contained a prominent triphenylphosphine signature, necessitating multiple chromatographic purifications. In the cases of 4-bromopyridine, the hydrochloride salt was used because of stability issues and was not totally soluble in the reaction solvents (THF and diisopropylamine (DIPA)), which could also have an adverse effect.

Molecular Orbital Plots. Molecular orbital plots of simplified structures of **1–9** (calculated with the Gaussian98¹⁴ suite of programs at the B3LYP/6-31G*¹⁵ level of DFT) are shown in Figure 4, with NBu₂ groups replaced with NMe₂. Similar to those for **12–14**,^{4a} the FMO plots of **1'–9'** indicate that most of the highest occupied molecular orbital (HOMO) density lies on the “donor” end of each chromophore, and much of the lowest unoccupied molecular orbital (LUMO) density lies on the “acceptor” end, irrespective of the particular substitution isomer. As with their analogue **14**, the *para*-substituted **3'**, **6'**, and **9'** show the most complete localization of the isosurface between the donor and acceptor units of the molecule; only a small amount of the LUMO density lies within the donor segments. As is shown by the MO plots, the overlap of the HOMO and LUMO on each compound is relatively small, occurring primarily at the central benzene ring. There is little to no overlap at the peripheries, indicating significant separation of the S₀ and first S₁ states. These results give good evidence of the intramolecular charge-transfer nature of the HOMO–LUMO transitions, and thus, the optical data should provide useful information about their potential as nonlinear optical materials. It is worth noting that more of the LUMO density lies on the central arene ring of **1'–9'** than in **12–14**, which may support the hypothesis that the charge-transfer efficiency can in fact be “tuned” by adjusting the strength of the acceptor group. It is also somewhat surprising that **4'–6'** show nearly as much FMO separation as **1'–3'** and **7'–9'**, even though the acceptor nitrogens are not situated to accept electron density via resonance. The efficiency of these partially inductive systems expands the library of possible acceptors even further. One or more trifluoromethyl groups appended to the acceptor arene segments, for example, may display similar behavior, as well as prove more chemically stable.¹⁶

(10) (a) Huang, J.-H.; Wen, W.-H.; Sun, Y.-Y.; Chou, P.-T.; Fang, J.-M. *J. Org. Chem.* **2005**, *70*, 5827–5832. (b) Yamaguchi, Y.; Kobayashi, S.; Wakamiya, T.; Matsubara, Y.; Yoshida, Z. *Angew. Chem., Int. Ed.* **2005**, *44*, 7040–7044.

(11) (a) Marsden, J. A.; Palmer, G. J.; Haley, M. M. *Eur. J. Org. Chem.* **2003**, 2355–2369. (b) Jones, C. S.; O'Connor, M. J.; Haley, M. M. In *Acetylene Chemistry: Chemistry, Biology, and Material Science*; Diederich, F., Stang, P. J., Tykwinski, R. R., Eds.; Wiley-VCH: Weinheim, 2005; pp 303–385. (c) Spitler, E. L.; Johnson, C. A., II; Haley, M. M. *Chem. Rev.* **2006**, published online Sep 19, 2006; <http://dx.doi.org/10.1021/cr050541c>.

(12) (a) Marsden, J. A.; Haley, M. M. In *Metal-Catalyzed Cross-Coupling Reactions*, 2nd ed.; de Meijere, A., Diederich, F., Eds.; Wiley-VCH: Weinheim, 2004; pp 317–394. (b) Sonogashira, K. In *Metal-Catalyzed Cross-Coupling Reactions*; Diederich, F., Stang, P. J., Eds.; Wiley-VCH: Weinheim, 1998; pp 203–230.

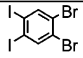
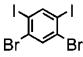
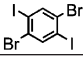
(13) (a) Haley, M. M.; Bell, M. L.; English, J. J.; Johnson, C. A.; Weakley, T. J. R. *J. Am. Chem. Soc.* **1997**, *119*, 2956–2957. (b) Bell, M. L.; Chiechi, R. C.; Johnson, C. A.; Kimball, D. B.; Wan, W. B.; Weakley, T. J. R.; Haley, M. M. *Tetrahedron* **2001**, *57*, 3507–3520.

(14) Gaussian 98, Revision A.6: Frisch, M. J.; Trucks, G. W.; Schlegel, H. B.; Scuseria, G. E.; Robb, M. A.; Cheeseman, J. R.; Zakrzewski, V. G.; Montgomery, J. A., Jr.; Stratmann, R. E.; Burant, J. C.; Dapprich, S.; Millam, J. M.; Daniels, A. D.; Kudin, K. N.; Strain, M. C.; Farkas, O.; Tomasi, J.; Barone, V.; Cossi, M.; Cammi, R.; Mennucci, B.; Pomelli, C.; Adamo, C.; Clifford, S.; Ochterski, J.; Petersson, G. A.; Ayala, P. Y.; Cui, Q.; Morokuma, K.; Malick, D. K.; Rabuck, A. D.; Raghavachari, K.; Foresman, J. B.; Cioslowski, J.; Ortiz, J. V.; Stefanov, B. B.; Liu, G.; Liashenko, A.; Piskorz, P.; Komaromi, I.; Gomperts, R.; Martin, R. L.; Fox, D. J.; Keith, T.; Al-Laham, M. A.; Peng, C. Y.; Nanayakkara, A.; Gonzalez, C.; Challacombe, M.; Gill, P. M. W.; Johnson, B.; Chen, W.; Wong, M. W.; Andres, J. L.; Gonzalez, C.; Head-Gordon, M.; Replogle, E. S.; Pople, J. A. Gaussian, Inc., Pittsburgh, PA, 1998.

(15) Becke, A. D. *J. Chem. Phys.* **1993**, *98*, 5648–5652.

(16) (a) Nguyen, P.; Todd, S.; Van den Biggelaar, D.; Taylor, N. J.; Marder, T. B.; Wittman, F.; Friend, R. H. *Synlett* **1994**, 299–301. (b) Touloupe, M. F.; Collings, J. C.; Burke, J. M.; Batsanov, A. S.; Ward, R. M.; Albesa-Jove, D.; Porres, L.; Beeby, A.; Howard, J. A. K.; Scott, A. J.; Clegg, W.; Watt, S. W.; Viney, C.; Marder, T. B. *J. Mater. Chem.* **2005**, *15*, 690–697.

TABLE 1. Yields for Preparation of TAEs 1–9

haloarene	donor coupling	TMSA/2-bromopyridine coupling (pdt)	TMSA/3-bromopyridine coupling (pdt)	TMSA/4-bromopyridine coupling (pdt)
	70%	17% (1)	47% (4)	20% (7)
	89%	79% (2)	59% (5)	54% (8)
	89%	60% (3)	51% (6)	89% (9)

Electronic Absorption Spectra. The absorption spectra of the TAEs (Figure 5a–c and Table 2) provide some insight into the electronic structure of the systems. All display a characteristic pattern of two broad absorption bands between 350 and 500 nm. Lowest energy bands are described in Table 2, and the next higher bands are given in the Supporting Information.¹⁷ Comparison with the parent nonfunctionalized compound reveals significant broadening and large (~75 nm) red shifts and more moderate red shifts (~15 nm) relative to the tetradonor compound. Such bathochromic shifts upon donor/acceptor functionalization are indicative of intramolecular charge transfer.¹⁸ On the other hand, comparison with the nitro acceptor analogues **12–14** (Figure 5d) show sharper cutoffs (below 550 nm) for **1–8**, possibly due to the weaker pyridyl acceptor groups. This could indicate more $\pi-\pi^*$ character in the excited state. Another striking difference is the similarity of the lowest energy absorption band shapes among different substitution isomers. For **12–14**, what we choose to call the *para* isomer (here **14**, in which like groups are *para* to each other with respect to the central benzene ring) exhibits a very low-intensity charge-transfer band. This is explained by the lack of linear charge-transfer pathways from the donors to the acceptors. The *ortho* and *meta* isomers, however, both have linear charge-transfer pathways and show strong charge-transfer bands. In the weaker acceptor systems presented here, the substitution pattern seems to have little effect on the strength of the charge-transfer bands. This can be explained by the greater LUMO density on the central benzene ring for all compounds, leading to a less drastic separation of partial charges among isomers. Extinction coefficients average in the 30000–50000 M⁻¹ cm⁻¹ range, in good agreement with the nitro analogues. For all compounds, the trend for longest wavelength λ_{max} appears to be *ortho* < *meta* < *para*, with *para* isomers displaying the most red-shifted charge-transfer bands. The only deviation from this trend is seen in **1**, where the charge-transfer band overlaps the next highest wavelength band, and is thus only a shoulder, making exact determination of the λ_{max} difficult. We have also calculated dipoles for **1–9** at B3LYP/6-31G*, which consistently show an inverse relationship with longest wavelength λ_{max} : all *para* isomers are calculated as 0.00 D, and all *ortho* isomers are in the 8–13 D range. These trends agree with our previous data

(17) We note the presence of possible shoulders in the longest-wavelength bands of *ortho* isomers **4** and **7** around 435–440 nm. The weakness of these shoulders makes wavelength and extinction coefficient determination impossible. The trend in all compounds is two prominent peaks past 350 nm, with the lowest energy peak assigned as the charge transfer absorption. Thus, to make symmetric comparisons between isomers, we have assigned the quantifiable peaks in **4** and **7** as the relevant bands. In particular, **4** bears striking resemblance to **11**, whose previously published spectroscopic data lists the 414 nm absorption rather than the potential shoulder at ~435 nm as the lowest energy band. We thus retain that convention here.

(18) (a) Pak, J. J.; Weakley, T. J. R.; Haley, M. M. *J. Am. Chem. Soc.* **1999**, *121*, 8182–8192. (b) Sarkar, A.; Pak, J. J.; Rayfield, G. W.; Haley, M. M. *J. Mater. Chem.* **2001**, *11*, 2943–2945.

for **12–14**. A small solvatochromic effect was observed for all nine compounds: absorption spectra displayed charge-transfer bands that experienced an average ~5 nm blue shift in toluene, compared to CH₂Cl₂. This in itself is not very interesting, but comparison between the absorption and emission spectra reveal some dramatic differences.

Electronic Emission Spectra. The electronic emission spectra of **1–9** in both CH₂Cl₂ and toluene are shown in Figure 6 and summarized in Table 2. The most striking feature of these spectra is the strong solvatochromism exhibited. While for a given solvent the emission λ_{max} does not vary much between compounds, changing the solvent leads to a shift of about 40–65 nm.

This effect, which is not observed to such an extent in either **12–14** or analogous planarized donor/acceptor annulenes,^{4a} can be attributed in part to solvent stabilization of the charge-transfer excited state. A polarized excited state is more stabilized by a polar solvent than a nonpolar solvent, while the nonpolar ground state is relatively unaffected, leading to a significant narrowing of the transition band gap and, hence, a bathochromic shift in the absorption and emission spectra.¹⁹ In this case, the emission spectra show the most dramatic shifts. Further red-shifting is observed in MeOH (Figure 10 and Table 3). A possible explanation may be that the ground states of **1–9** are predicted to be much less polar than **12–14** or the annulenes. A less polar ground state should lead to a greater decrease in the S₀–S₁ transition energy (red shift) upon switching to a more polar solvent. It is interesting to note that **1–9** visibly fluoresce in CH₂Cl₂, whereas **12–14** do not. The visible fluorescence is clearly related to the acceptor strength. Stronger donors and/or acceptor groups lead to very charge transfer-like HOMO-LUMO transitions,^{8d,e,20} wherein fluorescence can be quenched in polar solvents. A weaker acceptor would exhibit a transition that is more $\pi-\pi^*$ -like in character and resemble the parent **10** and tetradonor **11**, which *do* strongly fluoresce in polar solvents. This effect is not due to formation of dimers or higher aggregates in solution: experiments reveal no observable concentration dependence of ¹H NMR chemical shifts or emission wavelength over a 100-fold concentration gradient (e.g., 0.13–13 mM). This parallels our previously published data concerning nitrophenyl analogues **12–14**: significant aggregation requires enforced planarization to the corresponding (dehydrobenzoannuleno)-benzene variants.^{4a} Overall, these results support the hypothesis that varying the acceptor strength allows us the ability to fine-tune the optical band gap.

(19) (a) Seo, J.; Kim, S.; Park, S. Y. *J. Am. Chem. Soc.* **2004**, *126*, 11154–11155. (b) Yam, V. W.-W.; Wong, K. M.-C.; Zhu, N. *J. Am. Chem. Soc.* **2002**, *124*, 6506–6507. (c) Hong, J. W.; Woo, H. Y.; Liu, B.; Bazan, G. C. *J. Am. Chem. Soc.* **2005**, *127*, 7435–7443. (d) Spange, S.; Prause, S.; Vilsmeier, E.; Thiel, W. R. *J. Phys. Chem.* **2005**, *109*, 7280–7289. (e) Gawinecki, R.; Trzebiatowska, K. *Polish J. Chem.* **2001**, *75*, 231–239.

(20) (a) Rogers, D. W.; Matsunaga, N.; Zavitsas, A. A.; McLafferty, F. J.; Liebman, J. F. *Org. Lett.* **2003**, *5*, 2373–2375.

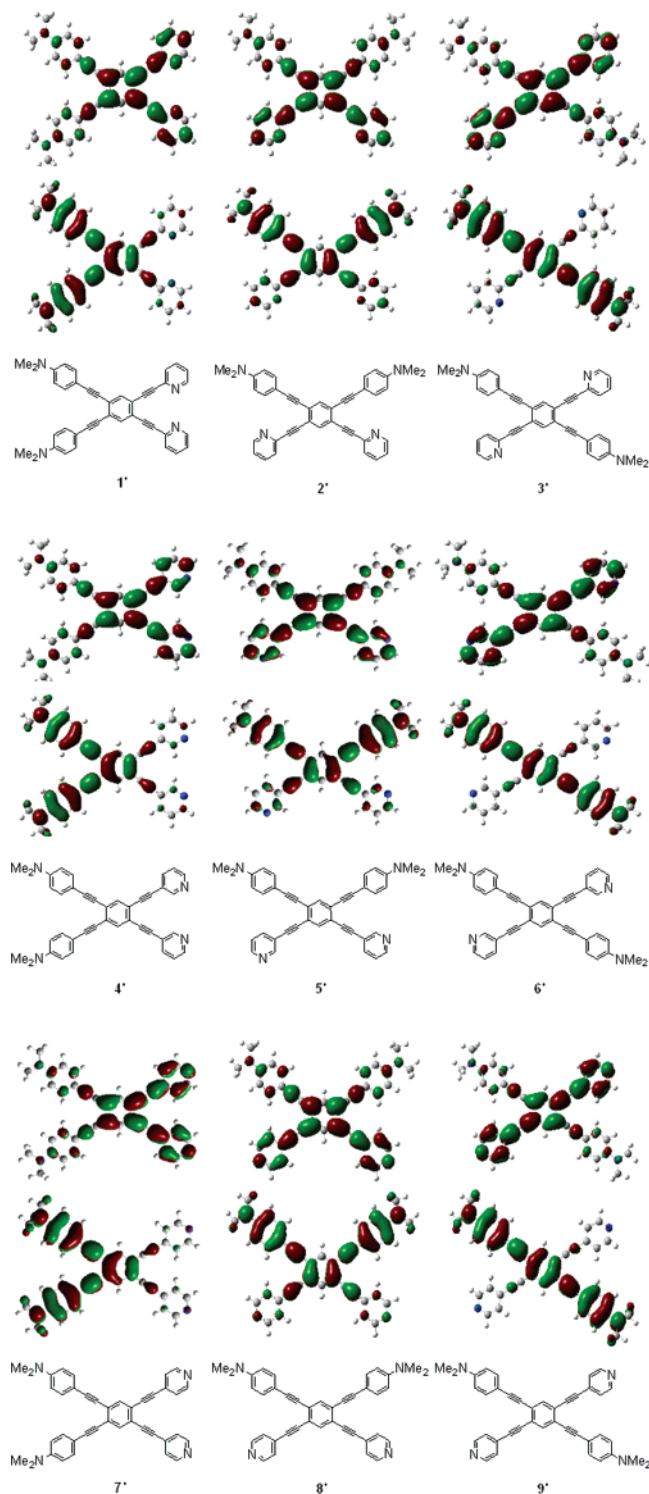


FIGURE 4. Molecular orbital plots (B3LYP/6-31G*) of simplified structures 1'–9'. The lower plots represent the HOMOs, and the upper plots represent the LUMOs.

Another structure–property question of interest was whether substitution isomer or nitrogen placement within the pyridine ring had the dominant effect on the optical properties of 1–9. Figure 7 shows the emission spectra of all nine isomers in CH₂Cl₂, expanded in the 520–580 nm region in order to examine each isomer's λ_{max} . It is clear that nitrogen placement within the pyridine ring (and hence the efficiency of the charge-transfer pathway at the termini) has a greater influence on fluorescence

wavelength red-shifting: when the acetylene linker chromophore is in the 3-position relative to the nitrogen, the emission has the shortest wavelength, and when the acetylene linker is at the 4-position, it has the longest. This trend holds true within each triad of compounds, and makes intuitive sense: the 2- and 4-ethynylpyridyl isomers both possess proper resonance forms for electron-transfer using arrow-pushing formalism, and the 4-ethynylpyridyl isomers in particular possess linear charge-transfer conduits. The 3-ethynylpyridyl isomers satisfy neither condition, and thus are closer in emission wavelength to the π – π^* transitions of the parent **10** and tetradonor **11**.

The fluorescence quantum yields for 1–9 in CH₂Cl₂ were calculated from the steady-state spectroscopic measurements using the techniques described by Drushel et al.²¹ The values are given in Table 2 and are also illustrated graphically in Figure 8, arranged in order of increasing acceptor strength. A noteworthy trend is the increasing quantum efficiency going from *ortho* to *meta* to *para* substitution isomer. This follows the trend in the longest wavelength λ_{max} in the absorption spectra, and Φ_f decreases as the calculated ground-state net dipole increases. Similarly, nitrogen placement within the ring has a significant effect: For a given substitution isomer, placing the nitrogen in the 3-position relative to the acetylene linker produced the largest Φ_f , and placement in the 4-position produced the smallest. The quantum yields of the all- π – π^* tetradonor system **11** and nitro acceptor analogues **12**–**14** were previously found to be 0.71 and >0.01 in CH₂Cl₂, respectively.^{4a} This data leads to the conclusion that the more π – π^* -like the system, the higher the fluorescence quantum yield. This is a well-established phenomenon, wherein decreased band gaps increase the accessibility of nonradiative de-excitation pathways via vibronic coupling.²² This can also help explain the fact that **9** does not follow the general trend seen in Figure 8: it is significantly red-shifted with respect to **7** and **8**, and hence, the decreased band gap is enough to lower the quantum yield more than the other isomers. Quantum yields in toluene were also determined, but there are no readily discernible trends. They are generally higher in toluene than CH₂Cl₂, though in some cases they are equal or lower. These results further indicate that solvent stabilization of the charge-transfer excited-state has a dramatic effect on the optical properties.

TFA Titrations. Recent work by Bunz and co-workers^{9,23} showed that donor/acceptor-functionalized aromatic cruciform structures (e.g., **18**, Figure 9) can serve as ion sensors via “switching” of intramolecular charge-transfer band gaps. Disrupting either the electron donor or acceptor has marked effects on the HOMO and LUMO energies, and protonation or complexation to metal ions represents a facile method of investigating the consequent structure-property implications. In the Bunz studies, protonation of the donor group of **18** with trifluoroacetic acid (TFA) in MeOH to pH = 2.7 led to a 161 nm hypsochromic shift (due to stabilization of the HOMO, thus widening the band gap), followed by a 105 nm bathochromic shift with further acidification to pH = 0.34, i.e., protonation of an acceptor group (stabilizing the LUMO, which narrowed

(21) Drushel, H. V.; Sommers, A. L.; Cox, R. C. *Anal. Chem.* **1963**, *35*, 2166–2172.

(22) (a) Tolbert, L. M.; Nesselroth, S. M.; Netzel, T. L.; Raya, N.; Stapleton, M. *J. Phys. Chem.* **1992**, *96*, 4492–4496. (b) Engelman, R.; Jortner, J. *Mol. Phys.* **1970**, *18*, 145–154. (c) Caspar, J. V.; Meyer, T. J. *J. Phys. Chem.* **1983**, *87*, 952–957.

(23) Gerhardt, W. W.; Zuccherro, A. J.; Wilson, J. N.; South, C. R.; Bunz, U. H. F.; Weck, M. *Chem. Commun.* **2006**, *20*, 2141–2143.

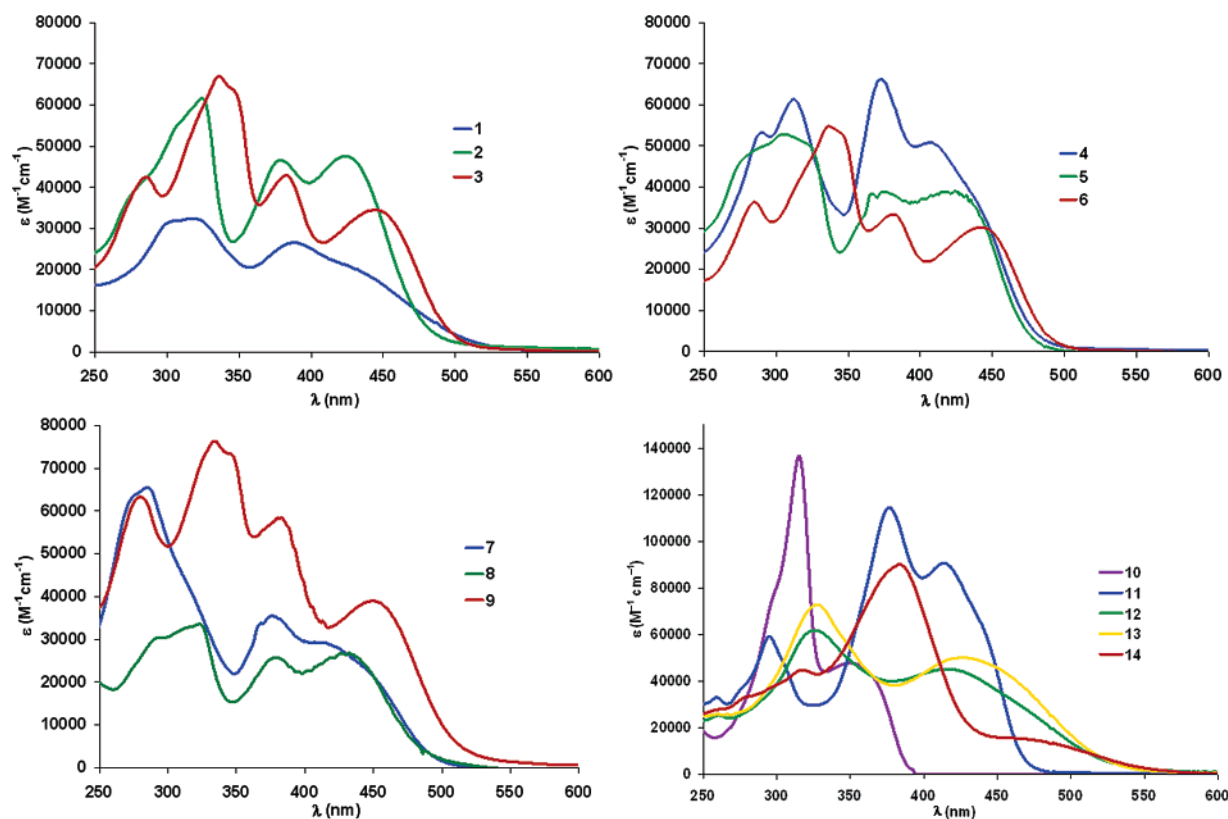


FIGURE 5. Electronic absorption spectra of (a) **1–3**, (b) **4–6**, (c) **7–9**, and (d) **10–14**. All spectra recorded in CH_2Cl_2 at analyte concentrations of 15–25 μM .

TABLE 2. Electronic Absorption and Emission Data and Calculated (B3LYP/6-31G*) Net Dipoles for TAEs **1–9**

compd	solvent	lowest energy abs λ_{max} (nm) (ϵ [$\text{M}^{-1}\text{cm}^{-1}$])	em λ_{max} (nm)	Stokes shift (nm)	Φ_{F}^b	net dipole (D)
1	CH_2Cl_2	435 ^a (21 000)	547	112	0.31	7.90
	PhMe	402 ^a (17 660)	482	80	0.63	
2	CH_2Cl_2	424 (47 540)	550	126	0.42	7.75
	PhMe	418 (35 680)	499	81	0.57	
3	CH_2Cl_2	446 (34 490)	550	104	0.49	0.00
	PhMe	437 (37 760)	508	71	0.47	
4	CH_2Cl_2	406 (50 920)	537	131	0.41	11.40
	PhMe	404 (50 030)	482	78	0.45	
5	CH_2Cl_2	424 (39 010)	547	123	0.47	6.50
	PhMe	416 (40 610)	488	72	0.49	
6	CH_2Cl_2	441 (30 210)	538	97	0.49	0.00
	PhMe	436 (29 780)	494	58	0.41	
7	CH_2Cl_2	407 (29 370)	558	151	0.20	13.10
	PhMe	407 (45 660)	499	92	0.20	
8	CH_2Cl_2	432 (26 820)	553	121	0.29	9.25
	PhMe	427 (29 640)	503	76	0.30	
9	CH_2Cl_2	449 (39 050)	558	109	0.27	0.00
	PhMe	440 (36 780)	512	72	0.38	

^a Approximate value as band is only a shoulder. ^b Calculated relative to fluorescein at pH = 8.

the band gap). This preferential protonation of the donor group first and then the acceptor group achieved a “switching” effect where shifting initially occurred in one direction, and then shifted back in the other direction with further addition of acid. Similarly, results by Fang and co-workers^{10a} indicate two-stage Hg ion sensing by **19**, which undergoes a 48 nm bathochromic shift in the absorption spectrum with exposure of up to ten equivalents of Hg^{2+} , followed thereafter by a 120 nm hypsochromic shift.

The structural similarity between **1–9** and **18** suggested that our systems might respond in an analogous manner. Each compound was titrated with TFA in MeOH, and the emission spectra recorded (e.g., Figure 10 for **2**; see Supporting Information Figure S1 for spectra of **1–9**). In every case, a large (average 172 nm) hypsochromic shift was displayed (Table 3) from the visible red region to borderline UV (Figure 11 inset). A significant increase in fluorescent intensity at each new λ_{max} was also exhibited. In general, the most hypsochromic state was achieved in each case at or around a TFA concentration of 10^{-2} M. TAEs **4–6** required a slightly more acidic environment, reaching their shortest wavelength maxima near $10^{-1.3}$ M TFA. This shifting was accompanied in the absorption spectra by a gradual loss of the intramolecular charge-transfer band (e.g., Figure 11). Further addition of TFA caused a bathochromic shift into the visible blue-green region. In examining the three-by-three array (Figure S1), several striking trends are obvious. TAEs **4–6** experience the least secondary shifting (ca. 31 nm), and **7–9** experience the most (average 85 nm). This makes intuitive sense, as **4–6** show the least communication through the conjugated pathways, leading to a less sensitive charge-transfer switching mechanism manifested in the fluorescence emission. The opposite is true for **7–9**. Another increase in relative fluorescent intensity is seen during the second shift for **7–9**, as well as for **1**, **4**, and **6**. This is in stark contrast to **18**, in which the quantum yield is ultimately cut in half upon full protonation.^{9b} An interesting trend is noticeable for **1–3**, where the final relative fluorescent intensity decreases going from the *ortho* to the *meta* to the *para* isomer. This trend has yet to be explained satisfactorily, but within each triad the *ortho* isomer seems to be the most “sensitive” to protonation, and so may be

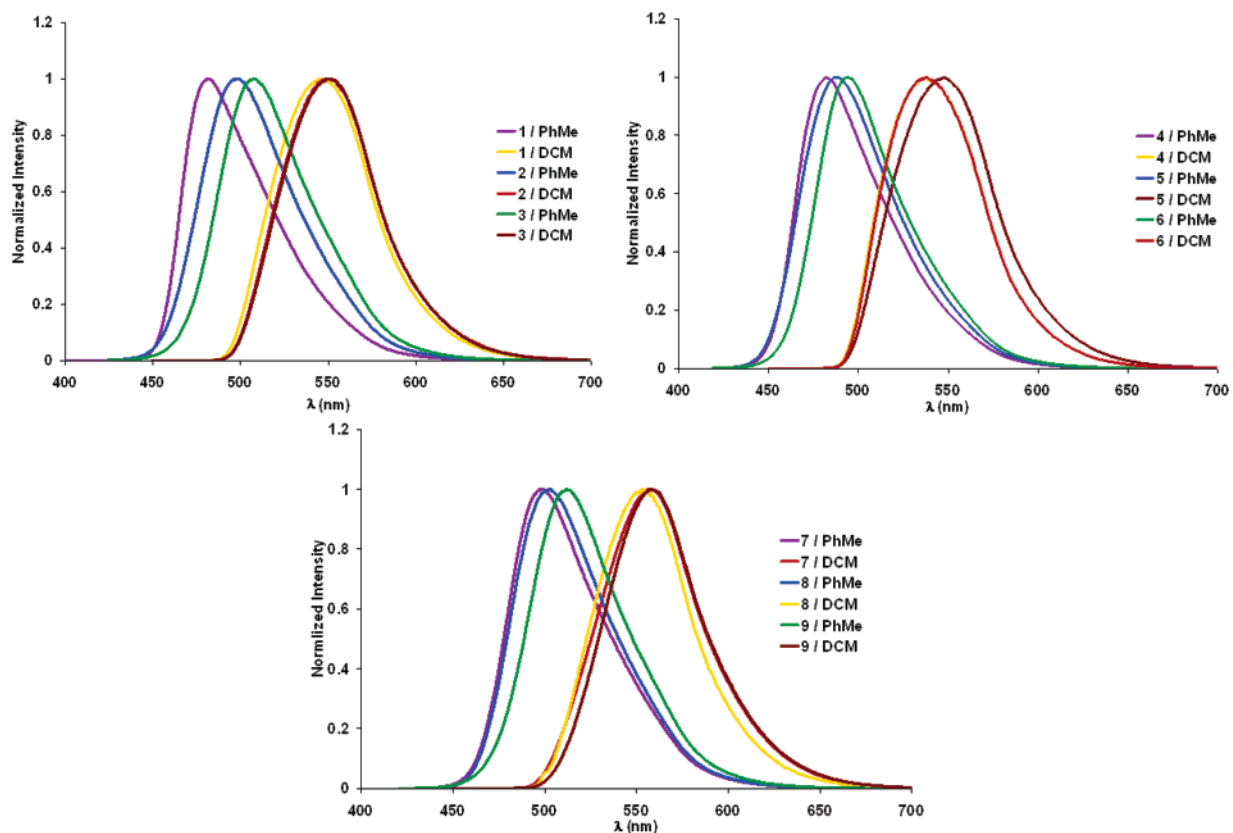


FIGURE 6. Emission spectra of (a) 1–3, (b) 4–6, and (c) 7–9 in CH_2Cl_2 (DCM) and toluene (PhMe). All spectra were recorded at analyte concentrations of 15–25 μM with excitation at the wavelengths of the lowest energy absorbance band of each (see Table 2).

TABLE 3. Summary of TFA-Induced Fluorescence Emission Shifting of TAEs 1–9

compd	initial λ_{em} (nm)	blue-shifted λ_{em} (nm)	red-shifted λ_{em} (nm)
1	566	388	468
2	564	390	472
3	561	393	464
4	561	390	422
5	557	388	418
6	560	388	419
7	569	391	488
8	567	391	476
9	572	413	485

related to the net dipole. Overall, these results support Bunz' findings that the donor nitrogens are protonated first, followed by the acceptor nitrogens. This is a surprising result, based on the expected relative $\text{p}K_{\text{a}}$'s of related compounds. Although diethylaniline has a $\text{p}K_{\text{a}}$ of 6.7 and pyridine a $\text{p}K_{\text{a}}$ of 5.3, our systems should more resemble expanded analogues of 4-(*N,N*-dimethylamino)pyridine (DMAP), in which the pyridine nitrogen is protonated first with a $\text{p}K_{\text{a}}$ of 9.2. The properties displayed both here and with **18**, therefore, represent rare if not unique behavior.

Zinc Ion Complexation. Bunz et al. also observed “switching” behavior upon complexation of Zn ion.^{9a,b} These authors used the similar response to protons and metal ions to discount the possibility of ion binding to the electron-rich aromatic π -face, in favor of binding directly to the nitrogens. Several efforts were made to reproduce this behavior in **1–9** using $\text{Zn}(\text{OTf})_2$ in CH_2Cl_2 ; however, the dramatic effect of protonation on our systems remained elusive when $\text{Zn}(\text{OTf})_2$ was used. No

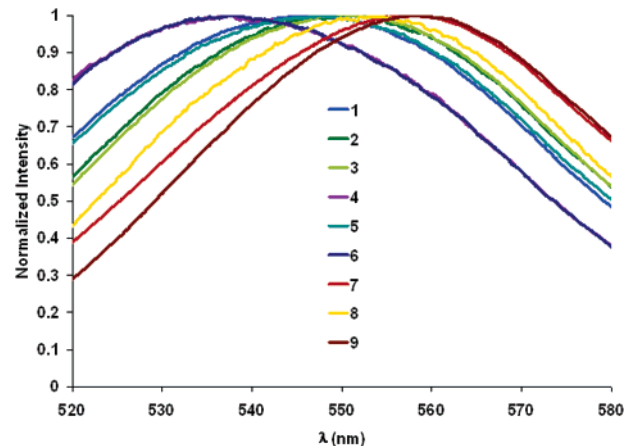


FIGURE 7. Emission spectra maxima of 1–9 in CH_2Cl_2 .

significant shifting activity was observed for any of the compounds under these conditions. It is possible that the Zn^{2+} ion may simply be too “soft” for efficient binding to the acetylene-based chromophores. Indeed, alkynes are often believed to confer less conjugation than olefins,²⁴ and it may be this fundamental structural difference between our compounds and **18** that causes the striking disparity in behavior. Using fluorescence quantum yield as a qualitative indicator of charge-

(24) (a) Rogers, D. W.; Matsunaga, N.; Zavitsas, A. A.; McLafferty, F. J.; Liebman, J. F. *Org. Lett.* **2003**, *5*, 2373–2375. (b) Rogers, D. W.; Matsunaga, N.; Zavitsas, A. A.; McLafferty, F. J.; Liebman, J. F. *J. Org. Chem.* **2004**, *69*, 7143–7417. (c) Jarowski, P. D.; Wodrich, M. D.; Wannere, C. S.; Schleyer, P. v. R.; Houk, K. N. *J. Am. Chem. Soc.* **2004**, *126*, 15036–15037.

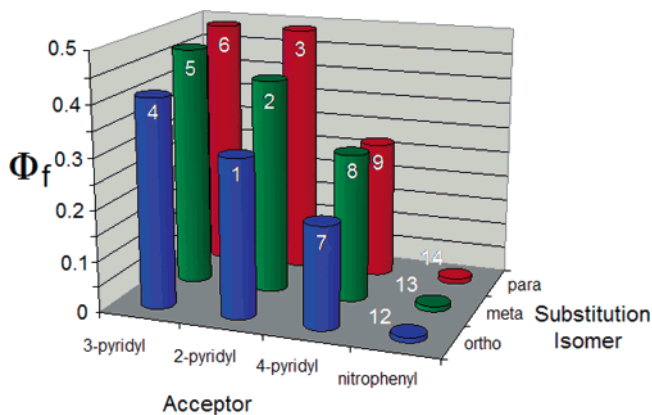


FIGURE 8. Graphical illustration of quantum yield trends for **1–9** and **12–14** in CH_2Cl_2 .

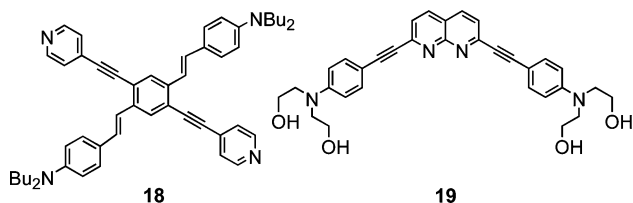


FIGURE 9. Donor/acceptor cruciforms **18** prepared by Bunz et al.⁹ and **19** by Fang et al.^{10a}

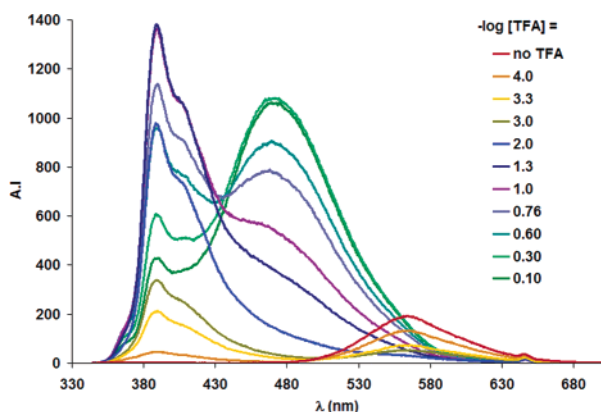


FIGURE 10. Example emission spectra of TFA titration of **2** in MeOH. The small peaks appearing in the spectra past 600 nm arise from interference by doubling of the excitation wavelength. Peaks from the excitation wavelength have been subtracted from each spectrum when necessary for clarity. All spectra were recorded at approximately $4 \mu\text{M}$ concentration. Excitation at most intense absorption peak (300–350 nm, present under all conditions).

transfer efficiency and conjugation supports this hypothesis: **1–9** exhibit quantum yields of ca. 0.20–0.50 in CH_2Cl_2 , whereas **18** has a quantum yield of 0.11 in the same solvent.

Efficient metal binding could potentially be promoted through the use of coordinating solvents such as THF. To help determine the effect of Zn^{2+} on **1–9** (e.g., Figure 12 for **1**; see Supporting Information Figure S2 for spectra of **1–9**), we exposed dilute ($\sim 0.4 \text{ mM}$) CH_2Cl_2 solutions of each compound to between 0.1 and 100 equiv of ZnCl_2 in CH_2Cl_2 diluted from a commercially available solution in THF and observed the change in the electronic emission spectra.²⁵ In each case, complexation produced an immediate bathochromic shift, as well as a quenching of fluorescent intensity. Red-shifting continued until approximately 1 equiv by up to 60 nm, but quenching continued

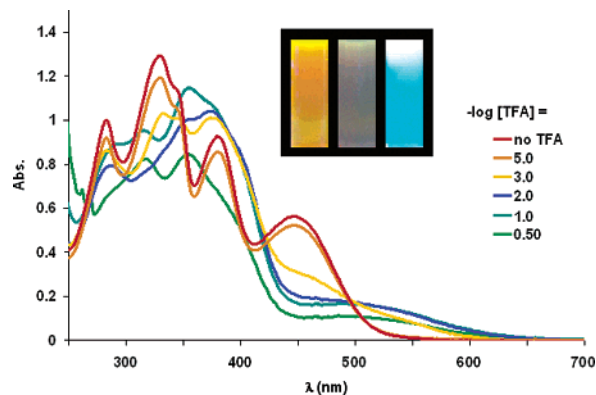


FIGURE 11. Absorption spectrum of TFA titration of **9** in MeOH at approximately $15 \mu\text{M}$ concentration. Inset: solutions of **9** in MeOH with no TFA (left) and at 10^{-2} M (middle) and $10^{-0.3} \text{ M}$ TFA (right); illumination by high-intensity 365 nm lamp.

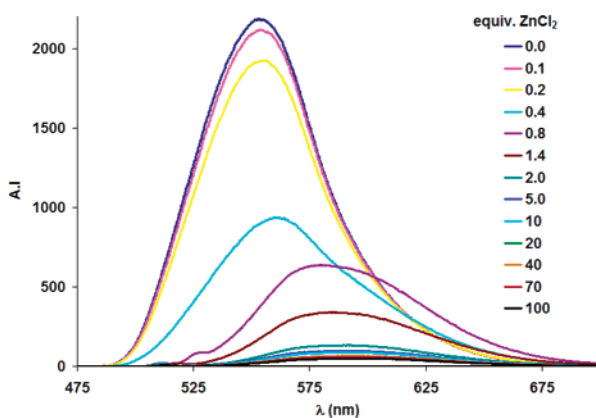


FIGURE 12. Example emission spectra of ZnCl_2 complexation to **1**. All spectra were recorded in CH_2Cl_2 at approximately 0.4 mM concentration. Small peaks appearing before 530 nm result from interference from the excitation wavelength. Excitation at the wavelength of lowest energy absorption peak (450–525 nm, present under all conditions).

until approximately 5–10 equiv of ZnCl_2 . During this period, the solutions of **4–6** fade from between green and yellow to cloudy and colorless. Although no particulates are visible, this may imply that nonfluorescent micro-aggregates of a high Zn: ligand complex are desolubilized. Upon addition of up to at least 100 equiv, fluorescent intensity returns at the new red-shifted wavelength, typically as a bright orange-red to deep red solution (note the contrast to the modest effect of ZnCl_2 in 100% CH_2Cl_2 , Figures 16 and 17). It is believed that as more Zn-containing solvent is added, the complex becomes re-solubilized. This behavior is puzzling and may reflect complex equilibria involving metal chelation mechanism(s). TAEBS **1–3** and **7–9** do not display this behavior, and experience only red-shifting and quenching, with no increase in fluorescence at the new wavelength with addition of up to 100 equiv of Zn^{2+} . The more efficient charge-transfer pathways in these compounds may cause more efficient binding to the Zn ions, precluding the more dynamic equilibria seen with **4–6**. Deep red solutions are formed in the cases of **7–9**, possibly due to enhanced com-

(25) Experiments involving metal ion complexation are described in terms of equivalents of complexing ion and TFA titration experiments in terms of proton concentration to most closely parallel the conditions of the Bunz studies.^{9b}

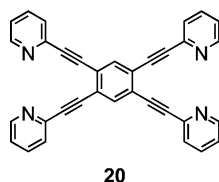


FIGURE 13. Tetrapyridyl ligand **20** prepared by Bosch et al.²⁶

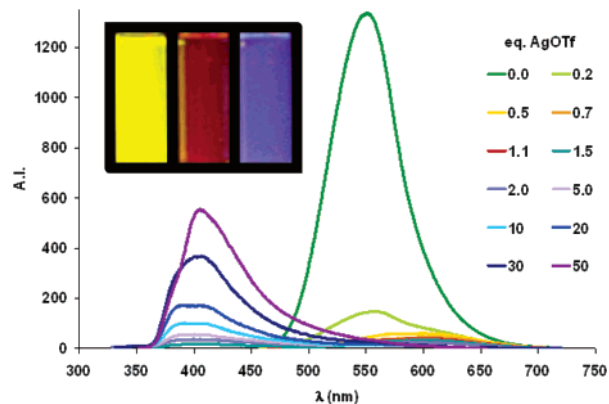


FIGURE 14. Emission spectra of addition of AgOTf to **1** in CH_2Cl_2 at approximately $12 \mu\text{M}$ concentration. Excitation at wavelength of most intense absorption band (300–350 nm, present in all compounds). Inset: solutions of **1** in CH_2Cl_2 with 0 (left), 1 (middle), and 50 (right) equiv of AgOTf; illumination by high intensity 365 nm lamp.

plexation through the more effectively conjugated 4-pyridyl ligands. It is also possible that these systems, potentially less-conjugated than **18**, experience ion binding through the aromatic π -faces, rather than the nitrogens directly. This sensitivity to specially solublized Zn ion may have potential for further development as fluorescent probes, especially given their additional pH-sensing properties. It should be stressed, however, that these results are necessarily qualitative in nature, and their greatest value is perhaps in illustrating the contrast in fundamental behavior upon minor structural alteration between our and Bunz's cruciform architectures.

Silver Ion Complexation. It has been shown that tetrakis-(2-pyridylethynyl)benzene (**20**, Figure 13) acts as an efficient bidentate ligand for Ag ions.²⁶ Crystal data revealed that AgOTf complexation to **20** enforces a conformation in which the nitrogens all point inward toward the Ag ions, with additional weak interactions between the triflate oxygen and the aromatic hydrogens at the 3-positions. With this in mind, we investigated the potential Ag(I) binding ability of **1**. It possesses the same structure as **20** at the acceptor end, with the donor electrons providing fluorescence. TAEB **1** was exposed to dilute AgOTf solutions in CH_2Cl_2 , and the emission spectra were recorded (Figure 14). An immediate bathochromic shift from 550 to 611 nm was observed, along with a precipitous drop off of fluorescent intensity. At 1 equiv of Ag ion, the analyte solution achieved a dark red color (Figure 14, inset). Additional AgOTf had much less effect as up to 50 equiv was required to cause the second, hypsochromic shift to a pale indigo color. As the (already low) peak at 611 nm disappears, the peak at 406 nm simultaneously grows more intense. In light of Bunz's findings, these results led to the extrapolative hypothesis that, in this case, initial binding of Ag ion is to the pyridine nitrogens in a

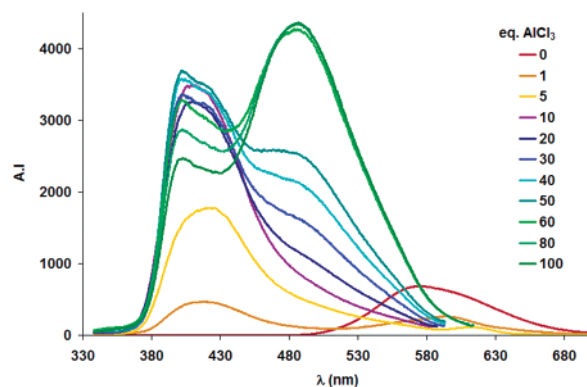


FIGURE 15. Example emission spectra of addition of AlCl_3 in MeOH to **9** at approximately $10\text{--}25 \mu\text{M}$ concentration. Peaks from $1\times$ and $2\times$ the excitation wavelength have been subtracted from each spectrum for clarity. Excitation at wavelength of most intense absorption band (300–320 nm, present under all conditions).

bidentate fashion, followed by the much less efficient subsequent binding to the donor nitrogens. This would have the effect of first stabilizing the LUMO, causing the red shift, and then stabilizing the HOMO, causing the blue shift. If the switching hypotheses are correct, it would seem that **1** represents a reverse-type sensor relative to **18**. Unfortunately, attempts at growing crystals of **1–9** either alone or in the presence of metal ions have been unsuccessful to date.

Aluminum Chloride Complexation. Due to the stark contrast between the effects of protonation and Zn ions on **1–9**, we next investigated the effect of a Lewis acid on the fluorescence. Each compound was exposed to solutions of AlCl_3 in MeOH, and the emission spectra were recorded (e.g., Figure 15 for **9**; see Supporting Information Figure S3 for spectra of **1–9**). Solvation to form $\text{Al}(\text{OMe})_3$ and protons produces a dynamic system involving both metal and acid that could be of interest. TAEBs **1**, **8**, and **9** showed response to $\text{Al}(\text{III})$ addition as a hypsochromic shift from 570 nm to ca. 395 nm with up to 10 equiv, followed thereafter by the generation of a third band at 475–490 nm. TAEB **7** showed the same behavior, but with initial appearance of the third band at as little as five equivalents. At 100 equiv, **7** displayed the most relatively intense middle band. Compound **1** exhibited much weaker behavior, with the middle band appearing only as a shoulder. TAEBs **2–6** did not show any such behavior, experiencing only a blue shift. This is presumably due once again to the inhibited conjugation caused by the position of the acceptor nitrogens. It is worth noting that the *ortho* isomers of both the 2- and 4-ethynylpyridyl triads showed the greatest amount of shifting. This may be due to the fact that they have the highest calculated dipoles and thus present more attractive targets for the ion. Bidentate chelation is not believed to be involved, since the pyridyl nitrogens in **7** are oriented away from each other, whereas in **1** they are oriented closer together. Bidentate binding should thus cause increased sensitivity in **1** relative to **7**, rather than the other way around. As in the case of the Zn complexation studies above, these results should only be considered qualitative in nature due to the ambiguity of the ions involved. They do, however, imply a certain generality in the fundamental basis of the switching mechanism.

Various Metals. The effect of various metal salts was investigated by taking **1**, **5**, and **9** as a representative cross-section of the compounds and exposing them to excess ions of different types (Figure 16). The three possible results are blue

(26) Bosch, E.; Schultheiss, N. *Cryst. Growth Des.* **2003**, *3*, 263–266.

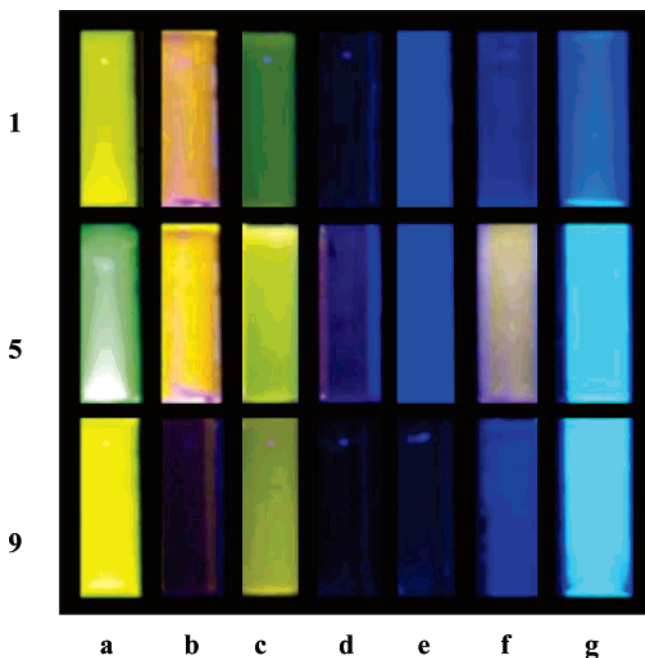


FIGURE 16. Effect of various metals on **1**, **5**, and **9** in CH_2Cl_2 : a, no ion; b, ZnCl_2 ; c, $\text{RuCl}_2(\text{bpy})_2$; d, $\text{PdCl}_2(\text{PhCN})_2$; e, AgBF_4 ; f, AgOTf ; g, AlCl_3 . Illumination by high intensity 365 nm lamp.

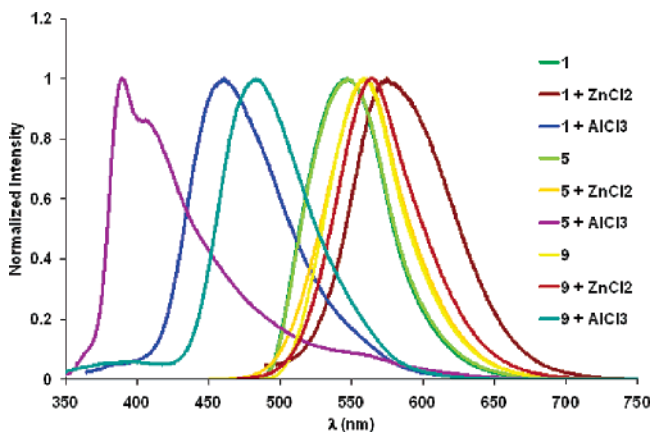


FIGURE 17. Normalized emission spectra of the effects of ZnCl_2 and AlCl_3 on **1**, **5**, and **9** in CH_2Cl_2 (columns b and g in Figure 16).

shifting of fluorescence, red shifting, or quenching. For **9**, quenching was the most common effect, with a blue shift upon exposure to AlCl_3 . TAEB **5** on the other hand retained its fluorescence most often. Excess ZnCl_2 (without coordinating THF in this case) quenched **9**, but only red-shifted **1** and **5**. Ag ions caused the most notable differences in response: while **1** and **5** were blue-shifted in AgBF_4 solution, TAEB **9** experienced quenching. While **1** and **9** experienced a blue shift in AgOTf , **5** was actually red-shifted as well as partially quenched. The differences produced by varying the counterion are thus illustrated. The differential responses imply the potential of **1–9** to form components of a “sensing array” for a host of applications.^{9,10a,27} Figure 17 provides a spectroscopic illustration of the effects of ZnCl_2 and AlCl_3 on **1**, **5**, and **9**.

Conclusions

Donor/acceptor systems **1–9** display a number of unique and interesting optical properties due to the weak pyridyl acceptor

group, including visibly fluorescent charge transfer, strong solvatochromism, and high quantum yields. These properties are not observed in the nitrophenyl acceptor-functionalized analogues we have previously reported.^{4a} The spectroscopic properties are susceptible to fine-tuning via small structural variations of the chromophore topography, providing access to a wide array of optical band gaps for customized optical materials applications. Emissive data support theories regarding band gaps and acceptor strengths; namely, that acceptor strength is inversely proportional to quantum yield, and that high quantum yields are available even with spatially separated frontier molecular orbitals.^{4a,9} Data for **4–6** in particular imply encouraging potential for inductively withdrawing electron acceptors, which we are currently investigating.²⁸ The TAEBs exhibit intramolecular charge-transfer switching via stepwise protonation in solution, providing support for the existing theory that the donor segment is more basic than the acceptor pyridines. This implies that spatially separate FMOs can be manipulated independently. Metal ion binding gives more complex data, and it is found that **1–9** bind stoichiometric amounts of Zn ion in solution only very weakly or not at all, in contrast to behavior reported for **18**.⁹ One possible contributor to this difference is the (possibly) less conjugation conferred by triple bonds versus double bonds.²⁴ AlCl_3 complexation provides data that is similar, but not identical to protonation, implying weak binding by the most conjugated compounds. Large excesses of the Al species produced intensely fluorescent solutions even in MeOH, in which quantum yields are expected to be low. This has potential consequences particularly in the area of OLEDs, which frequently contain Al ions.^{3b,c} Ag ion has a more impressive effect on **1**, first with likely bidentate chelation to adjacent pyridine nitrogens²⁶ followed by binding to the donor segments. This causes dramatic shifting in the emission spectra in a fashion that is the opposite of the effect of protonation. TAEBs **1–9** also respond differently to several different metal ions, providing potential as sensing arrays for a host of ions.^{9a,b,10a} Although the sensing effect is in some cases subtle, the high quantum yields of these weaker donor/acceptor systems may override sensitivity in overall attractiveness as materials components. We are currently using the insight attained herein to explore further functionalization options for maximization of the desirable optoelectronic properties, the results of which will be reported in the near future.

Experimental Section

General Alkyne Coupling Procedure A. Haloarene (1 equiv) and **16** (1.5 equiv per transformation unless otherwise noted) were dissolved in *i*-Pr₂NH/THF (1:1, 0.03 M) in a flask with KOH (aq, 50 wt %, 20 equiv). The solution was purged for 30 min with bubbling Ar followed by addition of $\text{Pd}(\text{PPh}_3)_4$ (0.03 equiv per transformation) and CuI (0.06 equiv per transformation). The reaction mixture was purged another 20 min and then stirred at rt for 12–48 h under an Ar atmosphere. Upon completion, the mixture was concentrated, rediluted with CH_2Cl_2 , and filtered through a pad of silica gel. The solvent was removed in vacuo, and the crude material was purified by column chromatography.

General Alkyne Coupling Procedure B. Donor-functionalized dibromoarene (1 equiv) was dissolved in *i*-Pr₂NH/THF (1:1, 0.05

(27) (a) Suslick, K. S.; Rakow, N. A.; Sen, A. *Tetrahedron* **2004**, *60*, 11133–11138. (b) Albert, K. J.; Lewis, N. S.; Schauer, C. L.; Sotzing, G. A.; Stitzel, S. E.; Vaid, T. P.; Walt, D. R. *Chem. Rev.* **2000**, *100*, 2595–2626. (c) Wiksur, S. L.; Ait-Haddou, H.; Lavigne, J. J.; Anslyn, E. V. *Acc. Chem. Res.* **2001**, *34*, 963–972.

(28) Spitzer, E. L.; Haley, M. M. Manuscript in preparation.

M) and the solution purged for 30 min with bubbling Ar. Pd(PPh₃)₄ (0.03 equiv per transformation) and CuI (0.06 equiv per transformation) were then added, and the solution was purged another 20 min. Trimethylsilylacetylene (TMSA, 1.5 equiv per transformation unless otherwise noted) was injected, and the solution was stirred at 65 °C for 12–48 h under an Ar atmosphere. Upon completion, the mixture was concentrated, rediluted with CH₂Cl₂, and filtered through a pad of silica gel. The solvent was removed in vacuo, and the crude material was carried on to the next step without further purification.

General Alkyne Coupling Procedure C. The tetrayne product from procedure B was dissolved in THF (0.04 M) and purged for 30 min with bubbling Ar. Acceptor haloarene (3 equiv per transformation unless otherwise noted) was dissolved in *i*Pr₂NH/THF (1:1, 0.7 M) with KOH (aq, 50 wt %, 20 equiv) and purged for 30 min with bubbling Ar. Pd(PPh₃)₄ (0.03 equiv per transformation) and CuI (0.06 equiv per transformation) were added to the second solution, which was then purged another 20 min. The protected donor alkyne was added under an Ar atmosphere via slow injection over 8 h to the acceptor haloarene solution. The mixture was stirred at 65 °C for 8–12 h. Upon completion, the mixture was concentrated, rediluted with CH₂Cl₂, and filtered through a pad of silica gel. The solvent was removed in vacuo, and the crude material was purified by column chromatography.

1,2-Dibromo-4,5-bis[(4'-*N,N*-dibutylaminophenyl)ethynyl]benzene (21). 1,2-Dibromo-4,5-diiodobenzene²⁹ (630 mg, 1.29 mmol) was reacted with donor alkyne **16**^{4a} (798 mg, 2.65 mmol) using general procedure A. The crude material was chromatographed on silica gel (4:1 hexanes/CH₂Cl₂) to yield **21** (622 mg, 70%) as a yellow oil. ¹H NMR (CDCl₃): δ 7.71 (s, 2H), 7.39 (d, *J* = 8.8 Hz, 4H), 6.57 (d, *J* = 8.8 Hz, 4H), 3.29 (t, *J* = 7.5 Hz, 8H), 1.58 (quin, *J* = 6.3 Hz, 8H), 1.37 (sext, *J* = 7.6 Hz, 8H), 0.96 (t, *J* = 7.6 Hz, 12 H). ¹³C NMR (CDCl₃): δ 148.6, 135.6, 132.4, 128.9, 123.0, 112.5, 108.4, 97.7, 85.2, 51.0, 29.7, 20.6, 14.3. IR (NaCl): ν 2197, 1602, 1606, 1519 cm⁻¹. MS (APCI): *m/z* ([isotope]) 762.8 (M⁺[⁷⁹Br⁸¹Br] + THF, 15), 760.8 (M⁺[⁷⁹Br⁷⁹Br] + THF, 26), 692.7 (M⁺[⁸¹Br⁸¹Br], 55), 690.8 (M⁺[⁷⁹Br⁸¹Br], 100), 688.7 (M⁺[⁷⁹Br⁷⁹Br], 48).

1,3-Dibromo-4,6-bis[(4'-*N,N*-dibutylaminophenyl)ethynyl]benzene (22). 1,3-Dibromo-4,6-diiodobenzene³⁰ (355 mg, 0.73 mmol) was reacted with donor alkyne **16** (450 mg, 1.49 mmol) using general procedure A. The crude material was chromatographed on silica gel (4:1 hexanes/CH₂Cl₂) to yield **22** (446 mg, 89%) as a red oil. ¹H NMR (CDCl₃): δ 7.81 (s, 1H), 7.63 (s, 1H), 7.38 (d, *J* = 9.0 Hz, 4H), 6.58 (d, *J* = 9.0 Hz, 4H), 3.29 (t, *J* = 7.8 Hz, 8H), 1.57 (quin, *J* = 8.7 Hz, 8H), 1.35 (sext, *J* = 7.6 Hz, 8H), 0.96 (t, *J* = 7.6 Hz, 12H). ¹³C NMR (CDCl₃): δ 148.6, 135.6, 134.0, 133.4, 125.9, 123.8, 111.4, 108.1, 97.4, 85.3, 51.0, 29.6, 20.6, 14.3. IR (NaCl): ν 2197, 1602, 1560, 1514, cm⁻¹. MS (APCI): *m/z* ([isotope]) 692.7 (M⁺[⁸¹Br⁸¹Br], 58), 691.7 (M⁺[¹³C⁷⁹-Br⁸¹Br], 40), 690.8 (M⁺[⁷⁹Br⁸¹Br], 100), 688.7 (M⁺[⁷⁹Br⁷⁹Br], 45).

1,4-Dibromo-2,5-bis[(4'-*N,N*-dibutylaminophenyl)ethynyl]benzene (17). 1,4-Dibromo-2,5-diiodobenzene³⁰ (1.41 g, 2.89 mmol) was reacted with donor alkyne **16** (2.00 g, 6.63 mmol) using general procedure A. The crude material was chromatographed on silica gel (4:1 hexanes/CH₂Cl₂) to yield **17** (1.77 g, 89%) as a red oil. Spectral data match those previously reported.³¹

1,2-Bis[(4'-*N,N*-dibutylaminophenyl)ethynyl]-4,5-bis(2-pyridylethynyl)benzene (1). TMSA (625 mg, 6.37 mmol) was coupled to **21** (1.50 g, 2.17 mmol) using general procedure B. The resulting red oil was coupled to 2-bromopyridine (1.96 g, 12.38 mmol) using general procedure C. The crude material was

chromatographed on silica gel (99:1 CH₂Cl₂/MeOH) to yield **1** (236 mg, 17%) as a dark red oil. ¹H NMR (CDCl₃): δ 8.92 (d, *J* = 5.8 Hz, 2H), 7.73 (t, *J* = 8.0 Hz, 2H), 7.66 (s, 2H), 7.60 (d, *J* = 8.0 Hz, 2H), 7.42 (d, *J* = 9.2 Hz, 4H), 7.35 (t, *J* = 5.8 Hz, 2H), 6.59 (d, *J* = 9.2 Hz, 4H), 3.30 (t, *J* = 7.5 Hz, 8H), 1.59 (quin, *J* = 6.9 Hz, 8H), 1.38 (sext, *J* = 7.0 Hz, 8H), 0.97 (t, *J* = 7.0 Hz, 12H). ¹³C NMR (CDCl₃): δ 150.3, 148.6, 143.5, 136.5, 135.1, 133.5, 128.0, 126.9, 123.6, 123.2, 111.4, 108.6, 98.3, 94.1, 87.7, 86.3, 51.0, 29.6, 20.6, 14.3. IR (NaCl): ν 3041, 2192, 1605, 1601, 1518 cm⁻¹. MS (APCI): *m/z* ([isotope]) 735.0 (M⁺, 100). UV (CH₂Cl₂) λ_{max} (log ε): 389 (4.45), 435 (sh, 4.32). Em λ_{max}: 547.

TFA Titration of 1–9. Solutions of **1–9** (35 μL, ~250 μM) were dissolved in spectrophotometric-grade MeOH (UV cutoff 204 nm) in four-sided quartz spectrophotometry cuvettes. Trifluoroacetic acid was diluted to concentrations ranging from 10⁻⁵ to 0.8 M in 10 mL MeOH. 2 mL aliquots were added to each solution of **1–9**. The solutions were capped and shaken, and the fluorescence spectra were then taken immediately.

Zinc Chloride Complexation to 1–9. Solutions of **1–9** (3.5 mL, ~0.4 mM) were dissolved in spectrophotometric-grade CH₂Cl₂ (UV cutoff 250 nm) in four-sided quartz spectrophotometry cuvettes. ZnCl₂ (0.5 M) in THF was diluted to 0.01 M with CH₂Cl₂, and between 0.10 and 100 equiv were injected via microsyringe. The solutions were capped and shaken, and the UV and fluorescence spectra were then taken immediately.

Aluminum Chloride Addition to 1–9. Solutions of **1–9** (3.5 mL, ~25 μM) were dissolved in spectrophotometric-grade MeOH (UV cutoff 204 nm) in four-sided quartz spectrophotometry cuvettes. Anhydrous AlCl₃ (0.021 g, 0.16 mmol) was dissolved in anhydrous MeOH (100 mL). Between 1 and 100 equiv of this 0.0016 M Al(III) solution were injected into the solutions of **1–9** via microsyringe. The solutions were capped and shaken, and the fluorescence spectra were then taken immediately.

Silver Triflate Addition to 1. A solution of **1** (3.5 mL, ~12 μM) was dissolved in spectrophotometric-grade CH₂Cl₂ (UV cutoff 250 nm) in a four-sided quartz spectrophotometry cuvette. Anhydrous AgOTf (0.0063 g, 0.025 mmol) was dissolved in anhydrous CH₂Cl₂ (10 mL) with vigorous sonication for 30 min. Between 0.2 and 70 equiv of this 0.0025 M Ag(I) solution were injected into the solution of **1** via microsyringe. The solutions were capped and shaken, and the fluorescence spectra were then taken immediately.

Addition of Excess Metal Salts to TAEBS 1, 5, and 9. Solutions of **1**, **5**, and **9** (5 mL, ~60 μM) were dissolved in spectrophotometric-grade CH₂Cl₂ (UV cutoff 250 nm) in 2 dram glass vials. Solid portions of each metal salt (at least 100 equiv each) were added to the vials. The vials were capped, shaken, and then sonicated for 1 h. The supernatant solutions were decanted from remaining solids (where applicable) into new vials, and the solutions were visualized under a high-intensity 365 nm lamp (Figure 16). Solutions containing no ion, ZnCl₂, and AlCl₃ were poured into four-sided quartz spectrophotometry cuvettes, and the spectra were taken.

Acknowledgment. We thank the National Science Foundation (CHE-0414175) for financial support. E.L.S. and L.D.S. acknowledge the NSF for IGERT fellowships (DGE-0114419). We thank Prof. O. H. Griffith for use of the fluorescence spectrophotometer and Prof. U. H. F. Bunz for helpful suggestions and for sharing results prior to publication.

Supporting Information Available: Experimental details and spectral data of **2–9**; copies of ¹H NMR spectra for **1–9**, **21**, and **22**; computational details; and emission spectra of **1–9** titrated with TFA or complexed with ZnCl₂ or AlCl₃. This material is available free of charge via the Internet at <http://pubs.acs.org>.

JO061712W

(29) Miljanic, O. S.; Vollhardt, K. P. C.; Whitener, G. D. *Synlett* **2003**, 29–32.

(30) Goldfinger, M. B.; Crawford, K. B.; Swager, T. M. *J. Am. Chem. Soc.* **1997**, *119*, 4578–4593.

(31) Tovar, J. D.; Swager, T. M. *J. Organomet. Chem.* **2002**, *653*, 215–222.